Modeling polystyrene homogeneous-coagulative nucleation in Pickering emulsion polymerization

Barthélémy Brunier, Yves Chevalier, Elodie Bourgeat-Lami, Nida Sheibat-Othman

Modeling polystyrene homogeneous-coagulative nucleation in Pickering emulsion polymerization

Barthélémy Brunier[1], Yves Chevalier[1], Elodie Bourgeat-Lami[2], Nida Sheibat-Othman[1]*

[1]Université de Lyon, Université Claude Bernard Lyon 1, CNRS, LAGEPP UMR 5007, 69616 Villeurbanne, France.

[2]Université de Lyon, Université Claude Bernard Lyon 1, CPE Lyon, CNRS, CP2M UMR 5128, 69616 Villeurbanne, France.

[*] Corresponding author: nida.othman@univ-lyon1.fr

KEYWORDS. Homogeneous coagulative nucleation; Population balance modeling; Hectorite clay platelets; Pickering surfactant-free emulsion polymerization.

ABSTRACT

Investigation of particle nucleation in surfactant-free emulsion polymerization of styrene using Laponite clay as Pickering stabilizer is considered. The effective number of clay platelets contributing to the surface charge of the polymer particles was calculated, and used to estimate their stabilizing efficiency. A coagulative nucleation mechanism was proposed and the coagulation coefficient was calculated using the DLVO theory. The Hamaker constant involved in the attractive potential of the clay-polymer composite particles was measured experimentally. The model was found to fit the experimental data in terms of the number of nucleated particles and the nucleation period. The effective number of clay platelets contributing to the surface charge was found higher than the number of platelets allowing full polymer latex surface coverage at the end of nucleation. Moreover, efficient stabilization against coagulation required almost complete coverage.

1. Introduction

Modeling of emulsion polymerization systems has attracted the attention of scientists for many years and models with different levels of complexity have been proposed to describe these systems.[1–6] Such models are not only useful for a better understanding of the underlying

reaction mechanisms but also allow optimization and control of the product quality and process conditions.[7–9]

Different stabilization systems have been proposed to prevent particle coagulation in conventional emulsion polymerization, using for instance anionic[10,11] or cationic[12,13] surfactants. Steric stabilizers can also be employed.[14,15] More recently, Pickering stabilization was considered using different types of inorganic particles, such as metal oxides (e.g., silica,[16–18] cerium oxide,[19] iron oxide[20]) or clay platelets[5,21,22] as solid stabilizers in view of the production of organic/inorganic colloidal nanocomposites. In such surfactant-free heterophase polymerization known as "Pickering emulsion polymerization", adsorption of the inorganic solid at the polymer particles surface is a key for ensuring efficient stabilization of the resulting latex suspension.

Among the variety of inorganic particles investigated so far, Laponite® clay has been found of particular interest.[5,23–31] Indeed, it presents the advantages of not requiring the use of auxiliary comonomers. The objective of the present work is to elucidate and model the nucleation and stabilization mechanisms taking place in the presence of Laponite® clay. Indeed, since the surface properties of Pickering latexes are different from those of polymer particles stabilized by surfactants, conventional emulsion polymerization models might not be valid. In a previous work, the effect of the layer of inorganic clay coating the polymer particles on radical capture was evaluated in seeded emulsion polymerization (where the number of particles was constant, so coagulation and nucleation were negligible).[32] The main results were the following: the pseudo-bulk model could be used to predict the particle size distribution since the particles were big enough (200 nm in diameter) to contain more than one radical at any given time or to make radical exit become negligible; Radical exit was estimated to be negligible for the considered particle size and reaction temperature (70 °C). Finally, radical capture was found to be proportional to the particle diameter and could be described by the diffusion-controlled mechanism with an efficiency factor of radical entry of $f_e = 0.014$, independent of the clay concentration, so no hindrance of radical capture resulted from the presence of clay at the polymer particle surface.

In the present work, we will focus on modeling the nucleation period. Nucleation is a determinant step in emulsion polymerization as it sets the number and size of particles, and hence, the reaction rate. In soap-free emulsion polymerizations, thus containing no surfactant micelles, it is commonly agreed that particle formation occurs through homogeneous coagulative nucleation, referred to as the Hansen-Ugelstad-Fitch-Tsai (HUFT) model of nucleation.[33,34] In this mechanism, primary latex particles are nucleated in the aqueous phase,

where the water-soluble initiator decomposes and produces primary radicals that grow through propagation reaction with monomer dissolved in water until reaching a critical chain length causing their precipitation. A first source of stabilization of these precursors is provided by the sulfate groups of absorbed radicals. If inorganic particles are present, they can, under certain conditions, strongly adhere to the surface of the formed precursors thus enhancing stabilization.[35] Then, precursor particles swell with monomer, absorb radicals from the aqueous phase and become the main loci of the polymerization. Homogeneous nucleation is usually followed by a limited coagulation process because the growth of particles and their concomitant increase of surface area makes the surface charge insufficient to ensure stabilization against coagulation. The precursor particles coagulate with each other, until the charge is high enough to stabilize the growing latex particles.

In this work, we report on the surfactant-free emulsion polymerization of styrene in the presence of Laponite® clay platelets as stabilizers, and potassium persulfate as initiator. The coagulative-nucleation mechanism is employed to describe the nucleation phenomenon, in which the Derjaguin-Landau-Verwey-Overbeek (DLVO)[36] theory is used to model the coagulation rate.[37] In this theory, repulsion between particles is governed by their surface charges, while the strength of van der Waals attractions is determined by the Hamaker constant and the particle size. The Hamaker constant is experimentally determined using turbidity measurements in provoked coagulation experiments. The effect of the clay concentration on the nucleation and coagulation rates is investigated.

2. Materials and methods

2.1. Materials

The monomer, styrene (Acros Organics, 99 % extra pure, stabilized) and the initiator, potassium persulfate (KPS, Sigma-Aldrich, minimum 99 %) were stored in a fridge until use. Hectorite clay under the brand Laponite® RDS was kindly donated by Rockwood additives (now BYK Additives Ltd). Deionized water of 18 MΩ·cm resistivity was used throughout the work. Sodium chloride (NaCl) was purchased from Sigma-Aldrich.

2.2 Emulsion polymerization experiments

A 1 L reactor was used with mechanical stirring at 400 rpm using a three blades Bohlender propeller. The polymerization reaction was performed in two successive periods: a first batch period for particle nucleation (formation of seed particles) followed by a second semi-batch

period for particles growth. The desired amount of clay powder (ranging from 0 to 10 g) was first dispersed in 800 g of water for 30 min under stirring in the reactor at ambient temperature. The resulting suspension was degassed using nitrogen flow and heated to 70 °C using a thermostated bath. Then, 40 g of styrene was added and the polymerization was initiated by adding 1.6 g of KPS (previously dissolved in about 20 g of water and degassed for 5 min). During the reaction, the stream of nitrogen was moved upwards off the reaction medium to the top of the reactor to maintain saturation of the gaseous atmosphere with nitrogen. At about 30 % conversion, the semi-continuous period was started by adding 160 g of monomer at a flow rate of 0.02 g s^{-1}. By this way, the polymer particles remain saturated with monomer, and there is no need to account for diffusion limitations in the model during a longer period. Samples were collected at specific time intervals to measure the solids content (SC, i.e. mass fraction of solid) by gravimetry and the particles size using dynamic light scattering (Zetasizer, Nano ZS, Malvern). The solids content was used to calculate the amount of polymer and the monomer conversion, after subtracting the mass of clay and initiator. Combination of both measurements allowed the calculation of the particle number. The surface coverage of the latex particles by the clay, θ, was estimated as the ratio of the area of the basal face of clay platelets, $N_c \pi r_c^2$ to the surface area of polymer particles, A_p, and assuming that there is no clay in the aqueous phase.[26] The number of clay platelets is calculated from the volume of clay introduced in the reaction medium assuming disc-like platelets, $N_c = m_c/(\pi r_c^2 h_c \rho_c)$, where m_c is the introduced mass of clay, ρ_c = 2570 kg·m^{-3} is the clay density,[38] $r_c = 28$ nm is the radius of the clay disc and $h_c = 1$ nm is its thickness.

2.3 Backscattering measurements – latex stability

The stability of the latex was assessed by means of light backscattering experiments using a Turbiscan Lab® Expert instrument equipped with a light source at 850 nm wavelength.[39–41] The measurement head was fixed at the middle height of the cell (at 25 mm from the bottom). The measurement cell is equipped with a three-blade impeller to maintain a homogeneous dispersion during salt addition (used at 1625 rpm). Backscattering was measured every second. Two latex samples were analysed: a latex produced with 1 g L^{-1} of clay with 254 nm in mean diameter with a final surface coverage by clay of about 10 %, and a latex produced with 2 g L^{-1} of clay with 240 nm in diameter with a final surface coverage of about 19 %. Both latexes were diluted to 5 wt. % solids content. Samples of 10 mL of the latex were placed in the turbidimeter cell, which was tuned at 25 °C. Scanning was started before adding salt, to acquire the

backscattering signal before coagulation. Then, a 300 µL aliquot of a sodium chloride solution (2 M) was added under stirring. Stirring was stopped immediately after completing the salt addition and the sample was monitored until stabilization of the backscattering signal. After each injection of salt, the signal decreased quickly and then stabilized on a plateau. Salt addition was repeated until almost no change in the backscattering signal was observed. The backscattering signal was normalized by the initial signal (before adding salt). A mean value was calculated for each injection of salt solution, once a plateau was reached (S_{salt}). Note that efficient agitation during salt injection is essential to ensure a uniform concentration of electrolyte instantaneously. However, as the agitation affects the backscattering signal, it must be stopped to record a correct measurement. The short agitation time is not expected to cause a significant shear to enhance orthokinetic coagulation. A reference sample was scanned in a similar way by adding only water, to estimate the effect of dilution on the backscattering signal (S_{w}). The backscattering signal of each sample was therefore corrected for the influence of dilution by adding the differential backscattering of the reference sample to which only water was added ($S = S_{\mathrm{salt}} + \Delta S_{\mathrm{w}}$).

The stability of the latex was assessed based on the change in the backscattering, which is provoked by adding a monovalent electrolyte (NaCl).[42] Indeed, the turbidity, τ, is function of the particle size and concentration (with $\tau = 1 - S$). Therefore, the change in the turbidity (and so the backscattering) can be correlated to a change in the particle size, if the solids content is kept constant. The experimental stability ratio can be calculated as the ratio of the rate of the change in turbidity in fast coagulation (i.e. when the electrolyte concentration, C_{e}, exceeds the critical coagulation concentration, *CCC*) to the rate of change in turbidity in slow coagulation:[43]

$$W = \frac{(\mathrm{d}\tau/\mathrm{d}t)_{\mathrm{fast}}}{(\mathrm{d}\tau/\mathrm{d}t)_{\mathrm{slow}}} \quad (1)$$

3. Modeling

3.1 Particle population balance

The comprehensive particle size distribution model in emulsion polymerization takes into account particle formation by nucleation, growth by polymerization and coagulation, through the following population balance equation (PBE):[44]

$$\frac{\partial F(r,t)}{\partial t} + \frac{\partial (F(r,t)G(r,t))}{\partial r} = R_{\mathrm{nuc}}(t)\delta(r - r_0) - R_{\mathrm{coag}}(r,t) \quad (2)$$

where $F(r,t)$ is the density of particles of radius between r and $r+\delta r$ at time t (part·dm^{-3} dm^{-1}), $G(r,t)$ is the growth rate of particles of size r (dm·s^{-1}), r_0 is the nucleation radius (dm), R_{coag} is the coagulation rate, R_{nuc} is the nucleation rate (part·dm^{-3} s^{-1}), and $\delta(r-r_0)$ is the Dirac delta function which is unity for $r=r_0$ and zero otherwise, which sets the boundary condition of the PBE:

$$F(r_0,t)=\frac{R_{\mathrm{nuc}}(t)}{G(r_0)} \tag{3}$$

The growth rate is given by:

$$G(r,t)=\frac{\mathrm{d}r}{\mathrm{d}t}=\frac{k_{\mathrm{p}}[M]^{\mathrm{p}}M_{\mathrm{m}}}{4\,\rho_{\mathrm{m}}N_{\mathrm{A}}\pi}\frac{\bar{n}(r,t)}{r^2} \tag{4}$$

where M_{m} is the monomer molar mass, ρ_{m} is the monomer density, k_{p} is the propagation rate constant, $[M]^{\mathrm{p}}$ is the concentration of monomer in the polymer particles and N_{A} is the Avogadro's number.[1]

3.2 Particle nucleation

In the present Pickering emulsion polymerization system, homogeneous coagulative nucleation is assumed to be the main particle formation mechanism as the system contains no micelles. Primary particles are assumed to be formed in water by precipitation of polymer chains initiated in water. These precursors get stabilized by the clay platelets dispersed in water. Limited coagulation may take place to reduce the surface area and ensure colloidal stabilization of a suitable number of particles. In coagulative nucleation, the rate of particle formation can be calculated from the rate of homogenous nucleation and formation of primary precursors based on the Hansen-Ugelstad-Fitch-Tsai theory (HUFT)[33,34] combined with the kinetics of coagulation of precursor particles using the Smoluchowski-Muller-Fuchs theory.[45,46] The coagulation rate coefficient can be calculated using the DLVO theory.

In the homogeneous nucleation mechanism, the creation of new particles in the aqueous phase occurs once the size of the oligomers reaches a critical value, j_{crit}, such that the decreased oligomer solubility in water causes their precipitation. The rate of formation of new particles by homogeneous nucleation is given by:

$$R_{\mathrm{hom}}(t)=k_{\mathrm{p_w}}[M]^{\mathrm{w}}\left[IM_{j_{\mathrm{crit}}}\right] \tag{5}$$

where $\left[IM_{j_{\mathrm{crit}}}\right]$ is the concentration of oligomers of size j_{crit}, $k_{\mathrm{p_w}}$ is the propagation rate coefficient and $[M]^{\mathrm{w}}$ is the monomer concentration, all in the aqueous phase. Nucleation kinetics are strongly related to the stabilization system and to the rate of coagulation during this period determining the rate of particle production.

3.3 Particle coagulation

Coagulation of latex particles may take place by perikinetic or orthokinetic mechanisms.[47] In Perikinetic coagulation, the frequency of collision between particles is determined by their Brownian motion. Electrostatic interactions take place when the colloidal particles have electrical charges.[48] Such charges may include ions formed by initiator decomposition present on the particles surface and those of the adsorbed stabilizer (DLVO forces), in addition to other possible non-DLVO forces (such as steric stabilization by adsorbed macromolecules, hydration in the electrical double layer and interactions between hydrophobic surfaces). Orthokinetic coagulation is due to fluid shear or gravity forces, which increase the frequency of particle collision and promote coagulation, while the efficiency of coagulation is determined by the same parameters as perikinetic coagulation. In this work, the effect of stirring on coagulation was evaluated experimentally and it was found that stirring did not affect the particles size or number, nor the reaction rate with the type of impeller considered and within the 200–400 rpm agitation speed range. Therefore, the contribution of orthokinetic coagulation was not considered.

3.3.1 Coagulation rate and kernel

Smoluchowski[45] proposed a model to describe the particle coagulation rate in colloidal suspensions:

$$R_{\mathrm{coag}}(r,t) = R^{+}(r,t) - R^{-}(r,t) \tag{6}$$

with R^{+} and R^{-} designing respectively the rates of particle appearance and disappearance by coagulation:[49]

$$\begin{cases} R^{+}(r,t) = \int_{r_0}^{\left(r^3-r_0^3\right)^{1/3}} \beta(r',r'',t)F(r',t)F(r'',t)\frac{r^2}{(r^3-r'^3)^{2/3}}\,\mathrm{d}r' \\ R^{-}(r,t) = F(r,t)\int_{r_0}^{\infty}\beta(r,r',t)F(r',t)\mathrm{d}r' \end{cases} \tag{7}$$

with $r'' = (r^3 - r'^3)^{1/3}$.

where β is the perikinetic coagulation kernel that describes the rate at which two particles of radii r and r' coagulate at time t (dm^3 part^{-1}·s^{-1}).[45] It can be expressed as a function of the Smoluchowski kernel combined to the stability ratio of particles (W) using Müller's equation:[50]

$$\beta(r,r') = \beta(r',r) = \frac{2k_{\mathrm{B}}T}{3\eta W(r,r')}\left(2 + \frac{r}{r'} + \frac{r'}{r}\right) \tag{8}$$

where η is the viscosity of the medium, k_{B} is the Boltzmann constant and T is the temperature.

3.3.2 Fuchs stability – DLVO theory

In the considered Pickering emulsion polymerization system, it is assumed that the polymer particles are stabilized by the charges of the initiator fragments as well as those of the clay platelets adsorbed on their surface. Steric stabilization by the clay is considered to be ineffective. Therefore, a coagulation kernel that only considers electrostatic interactions was used.

The most commonly used kernel in emulsion polymerization is based on the DLVO theory, which describes the coagulation of colloidal suspensions from the total energy of interaction of pairs of colloidal particles.[2,51] The total energy is the combination of electrostatic repulsive forces and dispersion attractive forces. Fuchs[46] studied the collision of particles undergoing Brownian motion in the presence of such interactions and defined the stability ratio as the inverse of the aggregation efficiency:

$$W(r,r') = (r+r')\int_{r+r'}^{\infty} e^{\left(\frac{V_T}{k_B T}\right)} \frac{dR}{R^2} \tag{9}$$

where R is the center-to-center distance separating two particles of swollen radii r and r', and V_T is the total potential energy given by the sum of attractive, V_A, and repulsive, V_R, potentials:

$$V_T = V_A + V_R \tag{10}$$

According to this theory, two particles can coagulate if the kinetic energy of their Brownian motion allows overcoming the potential barrier, which corresponds to the integral of the curve of the total potential with respect to the separation distance. Usually, the potential energy curve passes through a maximum ($V_{T,max}$) that the kinetic energy of the particles must exceed for particle aggregation to occur:[52]

$$W(r,r') \approx \frac{r+r'}{4\kappa r r'} e^{\left(\frac{V_{T,max}}{k_B T}\right)} \tag{11}$$

3.3.3 Attractive potential

The attractive potential is given by:

$$V_A = -\frac{A}{6}\left[\frac{2rr\prime}{R^2-(r+r\prime)^2} + \frac{2rr\prime}{R^2-(r-r\prime)^2} + \ln\left(\frac{R^2-(r+r\prime)^2}{R^2-(r-r\prime)^2}\right)\right] \tag{12}$$

where A is the Hamaker constant, that will be estimated in the following sections for the present system.

3.3.4 Repulsive potential

The repulsive potential can be obtained by the formula of Hogg, Healy and Fürstenau:[53]

$$V_{\mathrm{R}} = \frac{\pi\varepsilon r r'(\zeta^2+\zeta'^2)}{r+r'}\left[\frac{2\zeta\zeta'}{\zeta^2+\zeta'^2}\ln\left(\frac{1+e^{-\kappa L}}{1-e^{-\kappa L}}\right) + \ln(1-\mathrm{e}^{-2\kappa L})\right] \tag{13}$$

where $L = R - (r + r')$ is the edge-to-edge distance between particles, $\varepsilon = \varepsilon_0\varepsilon_{\mathrm{r}}$ is the relative permittivity of the medium, with ε_0 the vacuum permittivity and ε_{r} the water relative permittivity, and ζ is the electrokinetic potential of the particles at the shear plane:

$$\zeta = \frac{2k_{\mathrm{B}}T}{\nu e}\ln\left(\frac{\mathrm{e}^{\lambda_4}+1}{\mathrm{e}^{\lambda_4}-1}\right) \tag{14}$$

$$\lambda_4 = \delta_{\mathrm{s}}\kappa + \ln\left(\frac{\mathrm{e}^{\lambda_5}+1}{\mathrm{e}^{\lambda_5}-1}\right) \tag{15}$$

$$\lambda_5 = \frac{\nu e\psi}{2k_{\mathrm{B}}T} \tag{16}$$

where e is the electron charge, ν is the valence of counter ions, δ_s is the thickness of the Stern layer and ψ is the surface potential:

$$\psi = \begin{cases} \frac{r\sigma}{\varepsilon(1+\kappa r)} & \text{, if } \kappa r < 1 \\ \frac{2k_{\mathrm{B}}T}{e}\sinh^{-1}\left(\frac{e\sigma}{2\varepsilon\kappa k_{\mathrm{B}}T}\right) & \text{, if } \kappa r > 1 \end{cases} \tag{17}$$

where σ is the surface charge of the polymer particles. In this equation, if κr_s is greater than 1, the particle surface is approximately a flat surface, but if κr_s is less than 1, the contribution of the curvature of the particles cannot be neglected.

The inverse Debye length, κ, characterizes the thickness of the electrical double layer and the diffuse layer of the free ions of opposite charge to the particle surface:

$$\kappa = \sqrt{\frac{2e^2 N_{\mathrm{A}} I_{\mathrm{s}}}{\varepsilon k_{\mathrm{B}}T}} \tag{18}$$

where $I_{\mathrm{s}} = \frac{1}{2}\sum C_{\mathrm{e},i}\nu_i{}^2$ is the ionic strength, $C_{\mathrm{e,i}}$ is the concentration of ionic species i (initiator, stabilizer, electrolyte) and ν_{i} its ionic valence.

The total surface charge density of the polymer particles per unit surface area of polymer particles, σ, is due to the presence of charges of the initiator residues, q_{I}, and charged inorganic clay platelets, q_{c}, adsorbed on their surface:

$$\sigma = \frac{q_{\mathrm{c}}+q_{\mathrm{I}}}{A_{\mathrm{p}}} \tag{19}$$

The contribution of the ions formed by the initiator decomposition at time t is given by:

$$q_{\mathrm{I}} = 2(I(t_0) - I(t))\nu_{\mathrm{I}}\, eN_{\mathrm{A}} \tag{20}$$

where $I(t_0)$ and $I(t)$ are respectively the number of moles of initiator at initial time and at any time t, ν_{I} is the counter-ion valence of the initiator, and A_{p} is the total surface area of polymer particles per unit volume of latex:

$$A_{\mathrm{p}} = \int_{r_0}^{\infty} 4\pi r^2 F(r)\mathrm{d}r \tag{21}$$

The contribution of clay in the stabilization of this system (q_c) is unknown and will be estimated in the following sections.

3.4 Stabilizer partitioning

It was previously observed using a Quartz Crystal Microbalance that the adsorption of Laponite® RDS clay on the surface of a polystyrene film is very fast.[26] Moreover, multilayer arrangement of adsorbed clay platelets on the surface of the polymer particles was observed by transmission electron microscopy and validated by clay titration by Inductively Coupled Plasma Optical Emission Spectroscopy. Such measurements showed that there was almost no residual clay in the aqueous phase for all clay concentrations studied. Therefore, the amount of clay adsorbed on the polymer particles was taken as the total amount of clay introduced into the reactor.

3.5 Monomer and radical balances in the different phases

Other parts of the model required to predict different reactions and concentrations in the different phases can be found in the Supporting Information.[32,54] Note that these parts of the model are similar to conventional modeling of emulsion polymerization.

4. Results and discussion

The model presented above was used to estimate the particle size distribution during Pickering emulsion polymerization of styrene stabilized by clay platelets. The Hamaker constant involved in the attractive potential was first identified experimentally. Then, the complete model was employed and the contribution of the inorganic clay platelets to stabilization was evaluated.

4.1 Determination of the Hamaker constant

Figure 1 shows the evolution of the normalized backscattering signal ($S(t)/S(t_0)$) in the sample with 1 g L^{-1} clay. Each point in this curve corresponds to an injection of salt (obtained by averaging the obtained plateau after stabilization). Correction of the backscattering due to dilution is done based on a reference sample to which only water is added. At a constant solids content, the backscattering is known to decrease if the particle size increases (for particles bigger than about 300 nm). So, the observed decrease in the backscattering reveals an increase in particle size due to coagulation. Indeed, increasing the electrolyte concentration leads to the

compression of the electrical double layer (i.e. the Debye length becomes shorter). This weakening of electrostatic repulsions causes particle coagulation. The backscattering signal starts stabilizing after the injection of 0.14 mol·L^{-1} of salt, which corresponds to the *CCC*. The experimental stability ratio can then be calculated using the backscattering at the *CCC* as fast coagulation, as shown in Figure 2. A linear relation of $\log W$ is obtained as a function of $\log C_e$.[52] The figure confirms the intersection between fast and slow coagulation (which corresponds to the *CCC*) at about 0.14 mol·L^{-1} of salt. In the sample with 2 g L^{-1} clay, the *CCC* was about 0.17 mol·L^{-1}, so a slightly higher amount of electrolyte was required to completely coagulate the latex particles.

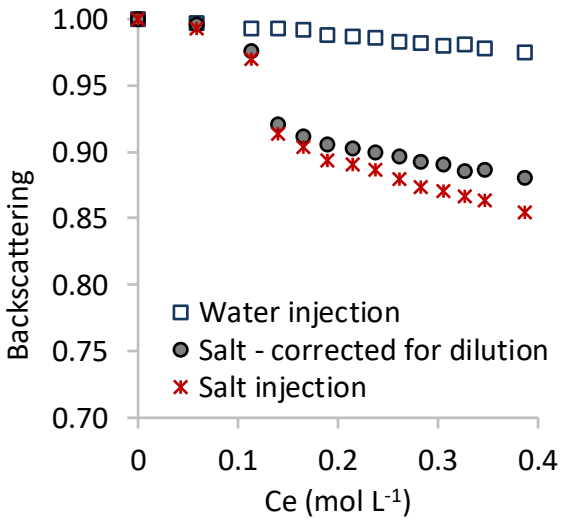

Figure 1: Evolution of the backscattering signal of a 5 wt % polystyrene latex (254 nm in diameter) armored with 1 wt% clay, upon several injections of electrolyte or only water.

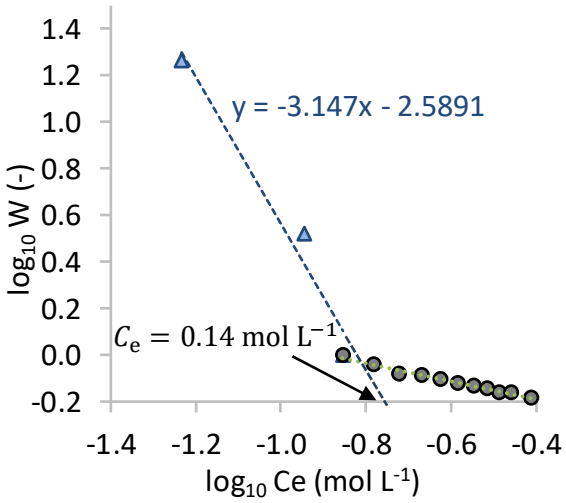

Figure 2: Estimation of the stability ratio based on the data in Figure 1.

The Hamaker constant, A, can be estimated from the experimental stability ratio by using the following correlation:[55]

$$A = \sqrt{\frac{1.73\times10^{-57}}{r^2 CCC}\left(\frac{\mathrm{d}\log W}{\mathrm{d}\log C_e}\right)^2} \qquad (22)$$

which gives $A = 0.28 \times 10^{-20}$ J for the sample with 1 g L^{-1} clay and $A = 0.15 \times 10^{-20}$ J for the sample with 2 g L^{-1} clay.

The Hamaker constant for detergent-free polystyrene particles varies over a wide range in the literature, $A = 0.1 - 1.5 \times 10^{-20}$ J (due to differences in the type of the used electrolyte and its possible chemical interaction with the surface of particles, the particle size and precision of the experimental method, the density of the surface charge groups, the dispersion medium, or the possible presence of some steric stabilization).[55,57] So, the identified Hamaker constant of the composite particles seems to be on a lower range compared to that of pure polystyrene latex, which would reveal a lower attraction potential, and hence a higher stability. But, the identified values are very close for the two samples with different clay concentrations. Note that other correlations exist to estimate the Hamaker constant based on the experimental stability ratio, leading to different results.[58,59]

The Hamaker constant can also be calculated theoretically, based on the refractive index (n) and the dielectric constant (ε), using the Lifshitz and Tabor-Winterton expression:[56]

$$A_{\mathrm{theo}} = \frac{3}{4}k_B T\left(\frac{\varepsilon_{r1}-\varepsilon_{r2}}{\varepsilon_{r1}+\varepsilon_{r2}}\right)^2 + \frac{3h\nu_e}{16\sqrt{2}}\frac{(n_1^2-n_2^2)^2}{(n_1^2+n_2^2)^{3/2}} \qquad (23)$$

where h is the Planck constant and v_e is the frequency of electron cloud oscillations, commonly estimated to be $v_e = 3 \times 10^{15}$ s^{-1}. Note again that other correlations exist for the calculation of the Hamaker constant theoretically.[60] For the clay, the refractive index $n_1 \approx 1.54$ and the dielectric constant (or relative permittivity) $\varepsilon_{r1} \approx 3.5$.[61,62] For polystyrene, $n_1 \approx 1.557$ and $\varepsilon_{r1} \approx 2.55$.[56] For water, $n_2 \approx 1.333$ and $\varepsilon_{r2} \approx 80$ [63] at ambient temperature. For clay platelets dispersed in water, the theoretical calculation gives $A_{\text{theo}} \approx 1.3 \times 10^{-20}$ J, and for polystyrene particles in water $A_{\text{theo}} \approx 1.55 \times 10^{-20}$ J. The clay dispersion is therefore more stable than the detergent-free polystyrene particles. The experimentally identified values of the Hamaker constant have a lower magnitude. Note that the experimentally identified Hamaker constant takes into account the presence of clay on the surface of polymer particles, the architecture of adsorption on the latex particles (where part of its charge may not be effective), besides possible stacking of clay platelets in water. It is therefore to be used in the DLVO model. The same value will be used ($A = 0.28 \times 10^{-20}$ J), independently of the clay concentration, as the identified constants were relatively close in the two samples. At last, it is worth noticing that the Hamaker constant is expected to increase only slightly with temperature.[60]

4.2 Estimation of the surface charge due to the clay

The clay can adsorb as multilayers on the polymer particles surface if the added amount of clay is higher than the amount required to ensure full coverage.[26] Therefore, only platelets adsorbed on the polymer particle that are directly in contact with water would contribute to the surface charge density of the polymer particles, while inner layers of platelets may not contribute to the surface charge. Consequently, the total surface charge due to the clay (q_c) is given by the product of the surface charge density of a single platelet (σ_0) and the effective number of platelets adsorbed on the polymer particles and in contact with water (N_c^{eff}):

$$q_c = N_c^{\text{eff}} \sigma_0 a_c \tag{24}$$

where a_c is the surface area of the face of a clay platelet ($a_c = \pi r_c^2$).

In the polymerization experiment performed with a clay concentration of 0.1 g·L^{-1}, the surface coverage was found to be the lowest, and decreases beyond 100 % during the first minutes of the polymerization. Therefore, interactions between the platelets adsorbed on the surface of the polymer particles can be neglected and the assumption of no multilayer adsorption can be made (the introduced amount is not sufficient to form more than one layer on the surface of polymer particles, assuming perfect dispersion of the clay in water at the beginning). In this case, all the

added clay actively contributes to the surface charge density of the polymer particle, i.e. $N_c^{eff} = N_c$. So, this experiment can be used to evaluate the surface charge density of one clay platelet, σ_0, which becomes the only unknown parameter in the model. The homogeneous nucleation model combined to the DLVO kernel coagulation were considered to describe nucleation in this Pickering system. In order to identify σ_0, its value was varied and the prediction of the particle number was compared to the experimental data. The resulting optimal value of surface charge density was $\sigma_0 \approx 0.2$ C m^{-2}. This value is higher than the literature for Laponite® RD clay platelets dispersed in water ($\sigma_0 = 0.048$ C·m^{-2}), which has a slightly different composition than RDS.[64]

4.3 Effective number of platelets contributing to the surface charge

The objective of this section is to predict the effective number of clay platelets on the surface of polymer particles in contact with water, N_c^{eff}, for the polymerization experiments carried out in the presence of increasing amounts of clay. The measured number of particles was compared to the model to fit the parameter N_c^{eff}. The simulation and experimental results are presented in Figure 3 for different clay concentrations. The nucleation period can be detected from Figure 3, and corresponds to the time period between the start of the experiment until the stabilization of the number of particles. It can be seen that the nucleation period increases with the clay concentration. With the lowest clay concentration (0.1 g L^{-1}), the nucleation period was about 20 minutes, while for the highest clay concentration, the number of particles continued to increase during more than one hour." For the experiments up to 3 g·L^{-1}, it was observed that the time when the number of particles stabilized corresponded to a surface coverage by the clay of about 100 %. This means that full coverage is required to stabilize the number of particles during the first moments, where the contribution of the initiator fragments in stabilization is still negligible. Then, the particles continue to grow and the surface coverage decreases up to 10 % in some cases, without further particle coagulation, as stabilization by the ions generated by initiator decomposition becomes significant. For the experiments with 5 g·L^{-1} and 10 g·L^{-1}, similar particle sizes were obtained and the surface coverage was higher than 100 % at the end of the nucleation period. This suggests that the generation of radicals of critical length in the aqueous phase becomes the limiting factor in particle generation.

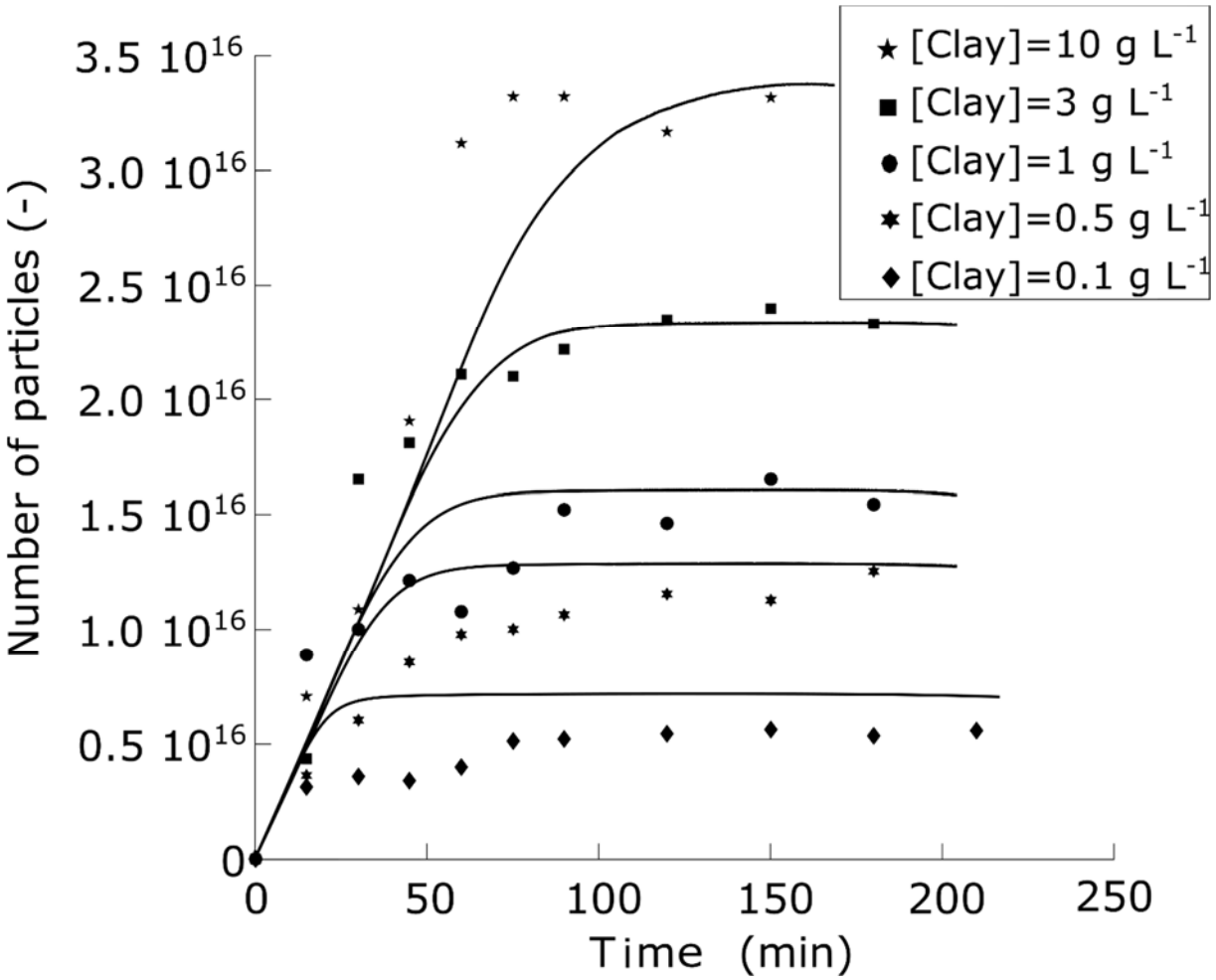

Figure 3: Estimation of the evolution of the particle number with time in Pickering emulsion polymerization of styrene for different clay concentrations, using N_c^{eff} as a fitting parameter. The continuous lines represent the model and the symbols the experimental data.

The individually estimated values of N_c^{eff} as a function of the clay concentration are shown in Figure 4. As expected, the number of clay platelets on the surface of the polymer particles increases when increasing the clay concentration, as almost all clay platelets are adsorbed on the polymer particles. However, the number of effective platelets contributing to polymer particle stabilization is not increasing linearly with the clay content. This can be explained by the fact that the clay is adsorbed as multilayers on the particle surface.[26] Upper layers may partly screen the charge of lower layers. It can be seen that for low clay concentrations (< 1 g·L^{-1}), all the clay platelets are contributing to the surface charge as the effective number of clay platelets is equal to the experimental one. Moreover, for such concentrations, the polymer particles were completely saturated by clay at the end of the nucleation period. For

clay concentrations higher than 3 $g \cdot L^{-1}$, only part of the clay was effectively contributing to the surface charge, as multiple layers of platelets start to be formed. An interpolation curve is indicated to predict the effective number of platelets as a function of the clay concentration. This allows modeling the nucleation phenomena without further fitting.

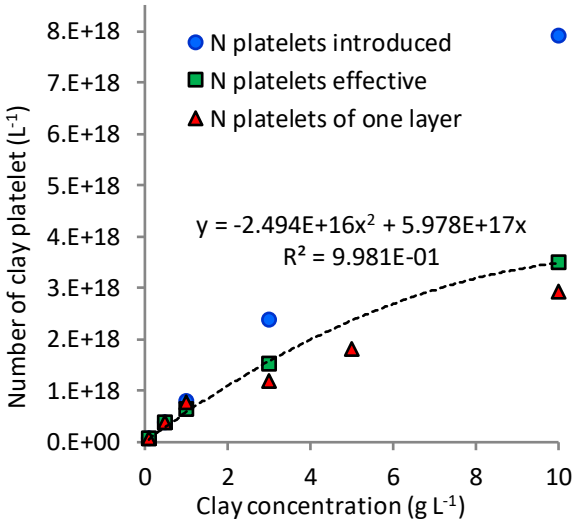

Figure 4: Number of platelets introduced in the system, compared to the number of platelets effectively contributing to the surface charge of the polymer particle and the number of platelets required to saturate the polymer particle with one clay layer at the end of nucleation. (--) Interpolation curve.

4.4 Evidence of coagulation during nucleation

Homogeneous nucleation presented in equation (5) was used either alone or combined to coagulation (i.e. coagulative nucleation) to predict the nucleated number of particles. Figure 5 shows that the number of particles created by homogeneous nucleation without coagulation was much higher than the measured one. By assuming homogeneous nucleation combined to coagulation in the model, a more realistic number of particles was estimated. This estimation is plausible, as a large number of precursors may be produced due to the high concentration of radicals and monomer in the aqueous phase. However, growth of these precursors would lead to a fast increase in their surface area, which would require a huge amount of stabilizer to prevent coagulation. The present amount of clay quickly adsorbs on the particle surface, but may not cover all the surface of precursor particles, especially with the increasing surface due to particle growth. In order to enhance their stability, precursor particles coagulate to reduce their surface tension. As mentioned above, the number of particles stabilized when the coverage

surface area by the clay attained about 100 %. Figure 6 shows that the model also fits well the prediction of the mean particle diameter. Finally, Figure 7 shows the evolution of the particle size distribution with time, where it is possible to detect a quick increase in the size of small particles at the beginning of the reaction due to the combined coagulation and growth phenomena. This is followed by particle growth at a lower rate as coagulation is significantly reduced for big particles. This simulation gives evidence for coagulation during nucleation that should therefore be taken into account in the model.

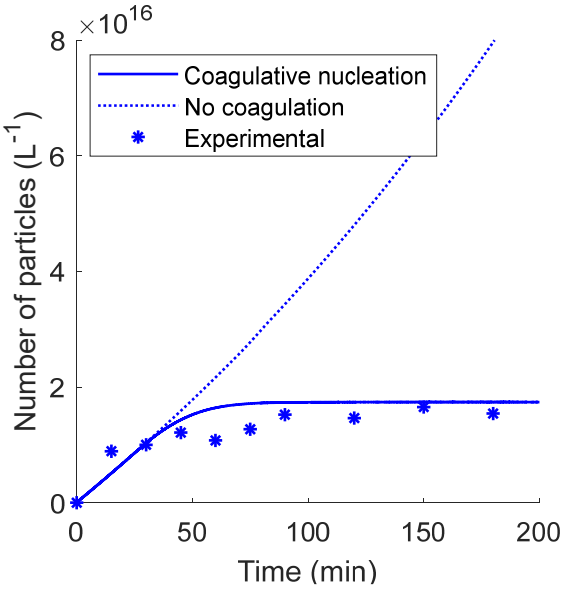

Figure 5: Evolution of the number of polymer particles in Pickering emulsion polymerization stabilized by 1 g L^{-1} of clay platelets. The model is evaluated either with coagulative nucleation or without coagulation.

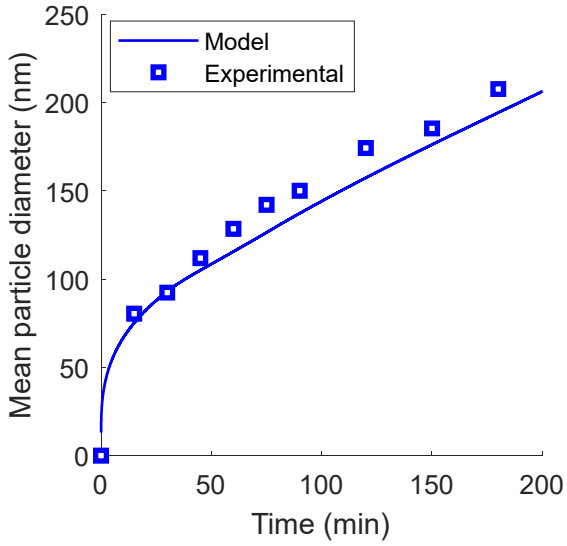

Figure 6: Evolution of the mean particle diameter in Pickering emulsion polymerization stabilized by 1 g L^{-1} of clay platelets

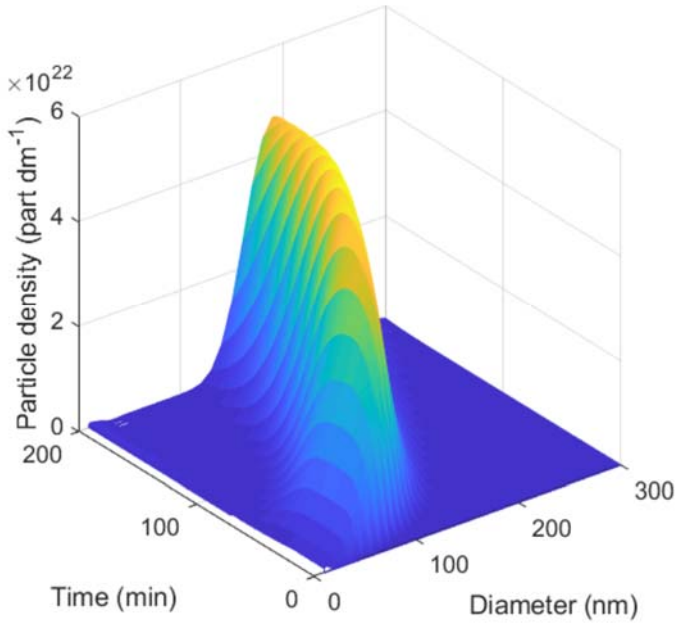

Figure 7: Evolution of the particle size distribution with time for Pickering emulsion polymerization stabilized by 1 g L^{-1} of clay platelets

5. Conclusions

In this work, a model was developed to predict the reaction kinetics in Pickering emulsion polymerisation where particle stabilization is ensured by clay platelets. The clay was found to have an important role in stabilizing polymer particles in surfactant-free emulsion polymerization. Smaller particles could be obtained when increasing the clay concentration, which led to a higher number of stabilized particles by the end of the reaction, at a given solids content. In order to describe this phenomenon, the coagulative-nucleation mechanism was assumed. Coagulation takes place in parallel to homogeneous nucleation. The DLVO theory was used to predict the coagulation coefficient. The Hamaker constant, characterizing the attractive potential of the composite particles, was estimated in provoked coagulation experiments.

Contrarily to surfactant-stabilized systems, clay platelets can form multilayers on the particle surface. This explains the nonlinear relationship between the total number of particles versus the clay concentration. Therefore, the stabilization efficiency of the clay is not straightforward to estimate as higher layers may partly screen the charge of lower layers. Therefore, the effective number of clay platelets contributing to the stabilization of the system was estimated experimentally and a relationship was proposed as a function of the clay concentration. The obtained model should be able the prediction of the rates of particle nucleation and coagulation as a function of the clay concentration.

6. Supporting information

The Supporting Information contains other details of the process model and a table with the used parameters.

Acknowledgement

The support of the Agence Nationale pour la Recherche is gratefully acknowledged (PickEP project, grant No. ANR-12-JS09-0007-01).

7. References

1. W. V. Smith, R. H. Ewart, *The Journal of Chemical Physics* **1948**, *16*, 592.

2. E. M. Coen, R. G. Gilbert, B. R. Morrison, H. Leube, S. Peach, *Polymer* **1998**, *39*, 7099.
3. S. C. Thickett, R. G. Gilbert, *Polymer* **2007**, *48*, 6965.
4. L. L. de Arbina, M. J. Barandiaran, L. M. Gugliotta, J. M. Asua, *Polymer* **1996**, *37*, 5907.
5. N. Sheibat-Othman, A. Cenacchi-Pereira, A. M. D. Santos, E. Bourgeat-Lami, *J. Polym. Sci. A Polym. Chem.* **2011**, *49*, 4771.
6. C. D. Immanuel, F. J. Doyle, C. F. Cordeiro, S. S. Sundaram, *AIChE J.* **2003**, *49*, 1392.
7. M. Alamir, N. Sheibat-Othman, S. Othman, *AICHE J.* **2010**, NA, doi:10.1002/aic.12148.
8. D. Edouard, N. Sheibat-Othman, H. Hammouri, *AICHE J.* **2005**, *51*, 3167.
9. T. J. Crowley, E. S. Meadows, E. Kostoulas, F. J. Doyle III, *J. Process Control* **2000**, *10*, 419.
10. D. Colombié, K. Landfester, E. D. Sudol, M. S. El-Aasser, *Langmuir* **2000**, *16*, 7905.
11. V. Castelvetro, C. De Vita, G. Giannini, S. Giaiacopi, *J. Appl. Polym. Sci.* **2006**, *102*, 3083.
12. J. Ramos, J. Forcada, *J. Polym. Sci. A Polym. Chem.* **2003**, *41*, 2322.
13. E. A. Zaragoza-Contreras, D. Navarro-Rodríguez, H. Maldonado-Textle, *J. Appl. Polym. Sci.* **2002**, *84*, 1513.
14. C. J. Ferguson *et al.*, *Macromolecules* **2005**, *38*, 2191.
15. N. Lazaridis, A. H. Alexopoulos, E. G. Chatzi, C. Kiparissides, *Chem. Eng. Sci.* **1999**, *54*, 3251.
16. P. J. Colver, C. A. L. Colard, S. A. F. Bon, *J. Am. Chem. Soc.* **2008**, *130*, 16850.
17. C. A. L. Colard, R. F. A. Teixeira, S. A. F. Bon, *Langmuir* **2010**, *26*, 7915.
18. N. Sheibat-Othman, E. Bourgeat-Lami, *Langmuir* **2009**, *25*, 10121.
19. I. Martín-Fabiani *et al.*, *ACS Appl. Nano Mater.* **2018**, *1*, 3956.
20. K. Li, P.-Y. Dugas, M. Lansalot, E. Bourgeat-Lami, *Macromolecules* **2016**, *49*, 7609.
21. E. Bourgeat-Lami, M. Lansalot, *Hybrid Latex Particles* **2010**, *233*, 53.
22. R. Ianchis *et al.*, *Appl. Clay Sci.* **2009**, *45*, 164.

23. E. Bourgeat-Lami, N. Sheibat-Othman, A. M. Dos Santos, *Polymer Nanocomposites by Emulsion and Suspension* **2010**, 269.
24. E. Bourgeat-Lami *et al.*, *Macromol. Symp.* **2007**, *248*, 213.
25. P. Aranda, E. Ruiz-Hitzky, *Acta Polym.* **1994**, *45*, 59.
26. B. Brunier, N. Sheibat-Othman, Y. Chevalier, E. Bourgeat-Lami, *Langmuir* **2016**, *32*, 112.
27. B. Brunier, N. Sheibat-Othman, M. Chniguir, Y. Chevalier, E. Bourgeat-Lami, *Langmuir* **2016**, *32*, 6046.
28. X. G. Qiao, P.-Y. Dugas, V. Prevot, E. Bourgeat-Lami, *Polym. Chem.* **2020**, *11*, 3195.
29. E. Bourgeat-Lami *et al.*, *Macromol. Rapid Commun.* **2010**, *31*, 1874.
30. L. Delafresnaye *et al.*, *Polym. Chem.* **2017**, *8*, 6217.
31. R. F. A. Teixeira, H. S. McKenzie, A. A. Boyd, S. A. F. Bon, *Macromolecules* **2011**, *44*, 7415.
32. B. Brunier, N. Sheibat-Othman, Y. Chevalier, É. Bourgeat-Lami, *AIChE J.* **2018**, *64*, 2612.
33. R. M. Fitch, C. H. Tsai, *Polymer Colloids* **1971**, 73, at <http://link.springer.com.docelec.univ-lyon1.fr/chapter/10.1007/978-1-4684-1920-7_5>.
34. F. K. Hansen, J. Ugelstad, *J. Polym. Sci. Polym. Chem. Ed.* **1978**, *16*, 1953.
35. **2014**, doi:10.1039/9781782620143.
36. B. Derjaguin, L. Landau, *Zhurnal Eksperimentalnoi I Teoreticheskoi Fiziki* **1945**, *15*, 663.
37. E. J. W. Verwey, J. T. G. Overbeek, **1948**.
38. B. Ruzicka, L. Zulian, G. Ruocco, *Langmuir* **2006**, *22*, 1106.
39. O. Mengual, *Talanta* **1999**, *50*, 445.
40. O. Mengual, G. Meunier, I. Cayre, K. Puech, P. Snabre, *Colloids and Surfaces A: Physicochemical and Engineering Aspects* **1999**, *152*, 111.
41. C. Chauvierre, D. Labarre, P. Couvreur, C. Vauthier, *Colloid Poly. Sci.* **2004**, *282*, 1097.
42. M. Fortuny, C. Graillat, T. F. McKenna, *Ind. Eng. Chem. Res.* **2004**, *43*, 7210.

43. B. Abismail, J. P. Canselier, A. M. Wilhelm, H. Delmas, C. Gourdon, *Ultrasonics Sonochemistry* **2000**, *7*, 187.
44. K. W. Min, W. H. Ray, *J. Macromol. Sci., Part C: Polym. Rev.* **1974**, *11*, 177.
45. M. v. Smoluchowski, *Z. Phys. Chem.* **1918**, *92U*, 129.
46. N. Fuchs, *Z. Physik* **1934**, *89*, 736.
47. N. Sheibat-Othman, H. M. Vale, J. M. Pohn, T. F. L. McKenna, *Macromol. React. Eng.* **2017**, *11*, 1600059.
48. A. S. Dunn, *Brit. Polym. J.* **1986**, *18*, 278.
49. C. D. Immanuel, F. J. Doyle III, *Chem. Eng. Sci.* **2002**, *57*, 4415.
50. H. Müller, *Kolloidchem Beih* **1928**, *27*, 223.
51. E. M. Coen, S. Peach, B. R. Morrison, R. G. Gilbert, *Polymer* **2004**, *45*, 3595.
52. H. Reerink, J. T. G. Overbeek, *Discussions of the Faraday Society* **1954**, 74.
53. R. Hogg, T. W. Healy, D. W. Fuerstenau, *Trans. Faraday Soc.* **1966**, *62*, 1638.
54. B. Brunier, N. Sheibat-Othman, S. Othman, Y. Chevalier, E. Bourgeat-Lami, *Can J. Chem. Eng.* **2017**, *95*, 208.
55. S.-L. Tsaur, R. M. Fitch, *J. Colloid Interface Sci.* **1987**, *115*, 463.
56. J. Israelachvili, **1992**.
57. R. H. Ottewill, *Emulsion polymerization* **1982**.
58. F. J. Rubio-Hernández, *Colloids and Surfaces A: Physicochemical and Engineering Aspects* **1994**, *88*, 141.
59. D. Bastos, F. J. de las Nieves, *Colloid Polym Sci* **1994**, *272*, 592.
60. R. Evans, D. H. Napper, *J. Colloid Interface Sci.* **1973**, *45*, 138.
61. P. Xu, T. Erdem, E. Eiser, *Soft Matter* **2020**, *16*, 5497.
62. P. B. Laxton, J. C. Berg, *J. Colloid Interface Sci.* **2006**, *296*, 749.
63. C. G. Malmberg, A. A. Maryott, **1956**, at <http://archive.org/details/jresv56n1p1>.

64. L. Li, L. Harnau, S. Rosenfeldt, M. Ballauff, *Phys. Rev. E* **2005**, *72*, 051504.